Surface-Chemistry Effect on Cellular Response of Luminescent Plasmonic Silver Nanoparticles

Shasha Sun,[†] Chen Zhou,[†,‡] Sishan Chen,[†] Jinbin Liu,[†] Jing Yu,[†] Jennifer Chilek,[†] Liang Zhao,[†] Mengxiao Yu,[†] Rodrigo Vinluan,[†] Bo Huang,[§] and Jie Zheng*,[†]

[†]Department of Chemistry, The University of Texas at Dallas, Richardson, Texas 75080, United States
[‡]School of Environmental, Physical, and Applied Sciences, University of Central Missouri, Warrensburg, Missouri 64093, United States
[§]Department of Pharmaceutical Chemistry, University of California, San Francisco, California 94158, United States

S *Supporting Information*

ABSTRACT: Cellular response of inorganic nanoparticles (NPs) is strongly dependent on their surface chemistry. By taking advantage of robust single-particle fluorescence and giant Raman enhancements of unique polycrystalline silver NPs (AgNPs), we quantitatively investigated effects of two well-known surface chemistries, passive PEGylation and active c-RGD peptide conjugation, on *in vitro* behaviors of AgNPs at high temporal and spatial resolution as well as chemical level using fluorescence and Raman microscopy. The results show that specific c-RGD peptide$-\alpha_v\beta_3$ integrin interactions not only induced endosome formation more rapidly, enhanced constrained diffusion, but also minimized nonspecific chemical interactions between the NPs and intracellular biomolecules

than passive PEGylation chemistry; as a result, surface enhanced Raman scattering (SERS) signals of c-RGD peptides were well resolved inside endosomes in the live cells, while Raman signals of PEGylated AgNPs remained unresolvable due to interference of surrounding biomolecules, opening up an opportunity to investigate specific ligand−receptor interactions in real time at the chemical level.
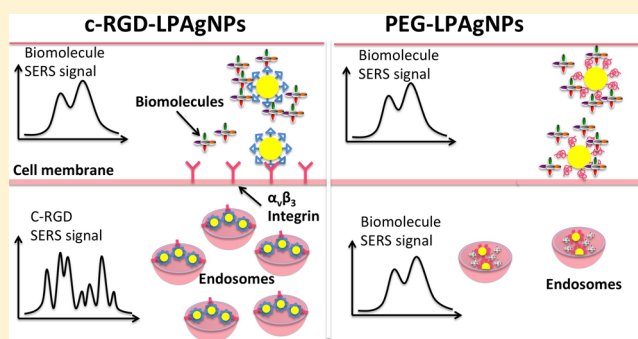
INTRODUCTION

Quantitative understanding of surface-chemistry effects on *in vitro* behaviors of inorganic nanoparticles (NPs) is of fundamental importance to their future success in preclinical research and clinical practices.[1−12] Two surface chemistries, PEGylation and conjugation of active targeting ligands such as cyclic Arg-Gly-Asp (c-RGD) peptides, have been widely applied to enhance the delivery of NPs into tumor sites.[8,13−15] With the assistance of PEG molecules, NPs can avoid macrophage uptake and passively accumulate in tumors at high efficiency through well-known enhanced permeability and retention (EPR) effect.[16−18] For instance, PEGylated gold NPs with a core size of ∼2.3 nm exhibited high tumor targeting efficiencies of 8.3 ± 0.9%ID/g at 12 h post injection (p.i.).[18] Gold nanocages coated with PEG surface ligand also enabled high blood retention and an efficient tumor uptake of 7.9 ± 1.1%ID/g at 24 h p.i.[17] Alternatively, conjugation of active targeting ligands that exhibit high affinities to cancer receptors is also a widely used strategy to increase tumor-targeting efficiencies of the NPs.[5,19] For example, c-RGD coated iron oxide NPs targeted integrin expressing tumor vasculature after injection, and a significant decrease of tumor magnetic resonance (MR) signal intensity (42 ± 5%) was observed.[20] While both surface strategies can enhance the tumor delivery of NPs at the *in vivo* level, how these two different surface chemistries quantitatively influence their follow-up cellular uptake, intracellular dynamics, and local chemical interactions inside endosomes still have not been fully understood and demand substantial investigations. To address these questions, NPs that not only exhibit robust single-particle fluorescence but also can chemically report local interactions are highly desired.

Luminescent plasmonic nanoparticles (LPNPs) are a class of nanofluorophores which can give bright and robust single-particle fluorescence while exhibiting plasmon properties such as strong surface plasmon absorption and large surface-enhanced Raman scattering (SERS) enhancements.[21−23] The synergy of these properties in one NP allows strengths of different optical microscopic imaging techniques to be integrated for better understanding of nano-bio interactions at the *in vitro* level. One strategy for creating such LPNPs is to coat a fluorescent quantum dot (QD) with an ultrathin gold nanoshell through precise control of the distance between QD
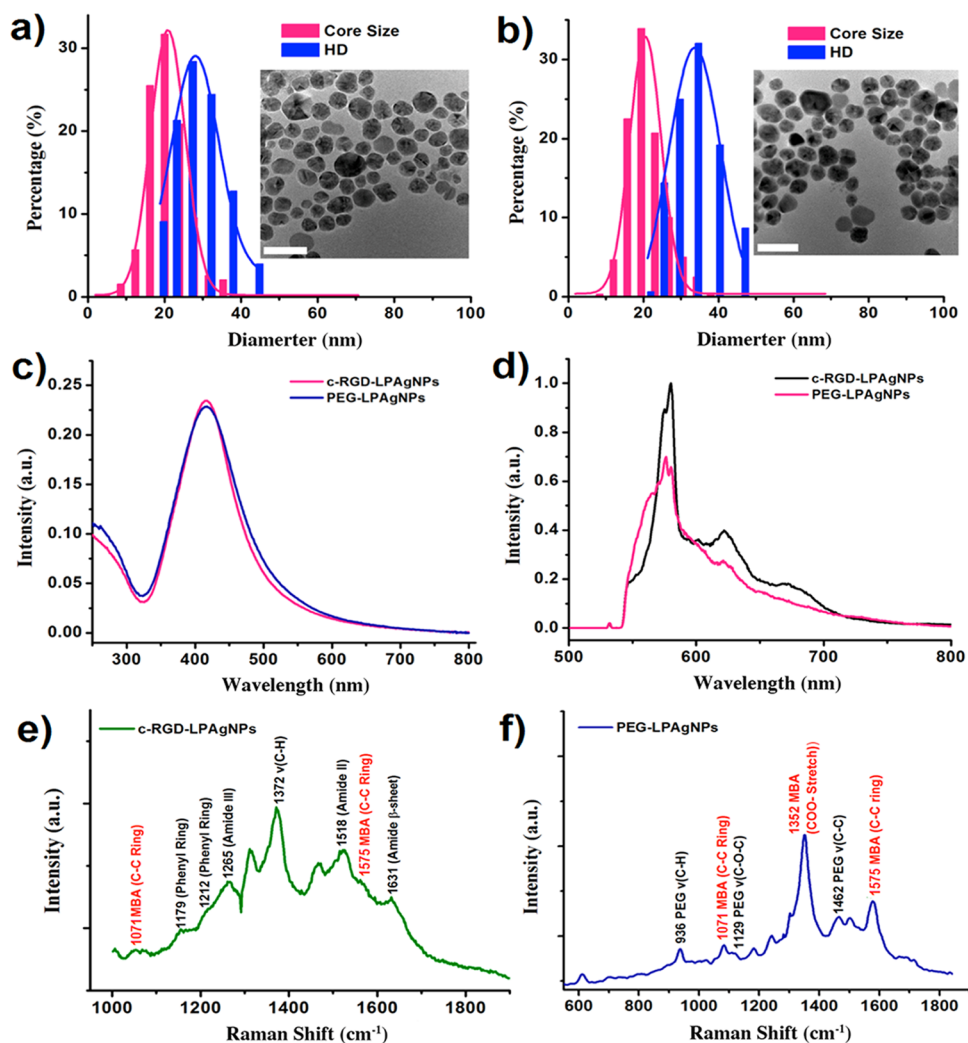
Figure 1. Characterization of LPAgNPs. (a) c-RGD-LPAgNPs with a core size of 20.9 ± 4.6 nm, and a hydrodynamic diameter (HD) of 28.1 ± 6.1 nm. (b) PEG-LPAgNPs with a core size of 20.5 ± 4.2 nm, and a HD of 33.7 ± 6.9 nm. The scale bar of the TEM images is 50 nm. (c) Absorption spectra of c-RGD-LPAgNPs and PEG-LPAgNPs. (d) Emission spectra of c-RGD-LPAgNPs and PEG-LPAgNPs. (e) Raman spectra of c-RGD-LPAgNPs. (f) Raman spectra of PEG-LPAgNPs.

and the shell with elegant surface chemistries.[22] Alternatively, by tuning grain size distributions of metal NPs, we were able to create 20 nm highly polycrystalline silver or gold NPs with strong single-particle fluorescence and giant Raman enhancements.[21,23] While simple cellular imaging of cancer receptors labeled with LPNPs has been demonstrated,[5,23] how to further apply them to advance our fundamental understanding of nano-bio interactions has not yet been demonstrated. In this communication, we applied luminescent plasmonic silver NPs (LPAgNPs) as contrast agents to quantitatively investigate the effects of two widely used surface chemistries in cancer targeting, passive PEGylation, and active c-RGD conjugation, on cellular uptake, intracellular dynamics, and local chemical interactions of the NPs inside the endosomes. Our studies showed that the conjugation of c-RGD peptides (Figure S1) to the NPs resulted in 20 times more rapid cellular uptake and also enhanced constrained motion of the NPs about 13% higher than that of PEGylation. In addition, specific binding between c-RGD and $\alpha_v\beta_3$ integrin minimized interference of intracellular biomolecules on Raman signals of LPAgNPs and allowed c-RGD vibrations to be well dissolved inside endosomes in the live cells, offering an exciting opportunity

to investigate ligand−receptor interactions in real time at the chemical level.

■ RESULTS AND DISCUSSION

The LPAgNPs with a mean size of ∼20 nm were selected for the follow-up bioconjugation and *in vitro* cellular studies. To conjugate c-RGD peptides or PEG molecules onto the particle surface, the LPAgNPs were incubated with mercaptobenzoic acid (MBA) and c-RGD peptides or 1 kDa PEG molecules. MBA ligand was introduced as the secondary ligand because its characteristic vibrations at 1071 cm^{-1} and 1575 cm^{-1} can serve as an internal standard during SERS studies. After the bioconjugation, the obtained NPs were further characterized with transmission electron microscopy (TEM) and dynamic light scattering (DLS). DLS studies showed that the hydrodynamic diameters (HDs) of the NPs coated with either c-RGD peptides or PEG molecules were 28.1 ± 6.1 nm (Figure 1a) and 33.7 ± 6.9 nm (Figure 1b) in phosphate buffer saline (PBS), respectively, indicating that NPs remained monodispersed in the physiological environment. HD layer of PEG-LPAgNPs (∼7 nm) was slightly larger than that of c-RGD conjugated ones (∼4 nm), indicating that PEG exhibited an

extended conformation once coated on the NP surface.[24] In addition, zeta potential measurements on these NPs showed that c-RGD-LPAgNPs and PEG-LPAgNPs were negatively charged in PBS buffer with zeta potentials of −30 mV and −32 mV, respectively. The obtained AgNPs retained their strong surface plasmons at 400 nm and exhibited identical absorption profiles, further suggesting that conjugation of the different ligands on the NP surface induced little change on their absorption (Figure 1c). Emission spectra of both PEG-LPAgNPs and c-RGD-LPAgNPs were composed of broad fluorescence background superimposed with sharp Raman emissions. Since PEG and c-RGD exhibit different Raman vibrational spectra, the overall emission spectra of AgNPs conjugated with different ligands exhibit different profiles (Figure 1d). The observation of Raman spectra from c-RGD-LPAgNPs and PEG-LPAgNPs also indicated that surface ligands were successfully conjugated on the NP surface. As shown in Figure 1e,f, Raman spectra of c-RGD-LPAgNPs showed the characteristic Raman vibrations of c-RGD ligands on the surface. For instance, the vibrations of amide β-sheet (1631 cm^{-1}), II (1518 cm^{-1}), III (1265 cm^{-1}), and phenyl ring (1179, 1212 cm^{-1}), of c-RGD were readily observed, consistent with the previous report.[25] Characteristic vibrations of PEG ligands on PEG-LPAgNPs such as the CH$_2$ rocking vibration (936 cm^{-1}), C−O−C asymmetric stretching (1129 cm^{-1}), the coupled vibration of C−C and C−O stretching (1132 cm^{-1}) and CH$_2$−CH$_2$ antisymmetric bending mode (1462 cm^{-1}) were also observed from PEG-LPAgNPs.[26] In addition, Raman bands of MBA on the LPAgNPs were observed at 1071, 1352, and 1575 cm^{-1}, which were exactly consistent with the previous report on C−C stretching ring-breathing modes (1071 and 1575 cm^{-1}) and COO stretching (1352 cm^{-1}), respectively.[27]

LPAgNPs with different surface ligands exhibited distinct binding affinities to glioblastoma U87MG cancer cells with high expression level of $\alpha_v\beta_3$ integrin receptors on the membrane. The fixed U87MG cancer cells were incubated with c-RGD-LPAgNPs and PEG-LPAgNPs of the same concentration (10 nM) in PBS respectively. After 45 min incubation, the excess amount of NPs was washed away with PBS and the cells were imaged under a fluorescence microscope with a 100× objective in total internal reflection geometry. As shown in Figure 2a,b, only a very small amount of PEG-LPAgNPs was found to nonspecifically bind to the U87MG cells because of the antifouling nature of PEG molecules.[8] On the other hand, a large amount of c-RGD-LPAgNPs was labeled on the cell membrane (Figure 2c,d). Because of a strong surface plasmon of c-RGD-LPAgNPs and their high-density labeling of U87MG cancer cells, the cells became yellowish and could even be readily observed with the naked eye (Figure S2). To further confirm that the observed high labeling efficiency of c-RGD-LPAgNPs was due to specific ligand−receptor interactions, we also conducted blocking and c-RAD peptide control studies. We first blocked the binding of the integrin receptors of U87MG cells with 1 mM c-RGD peptide and then incubated U87MG cells with c-RGD-LPAgNPs with the same procedures. No binding of the AgNPs with U87MG cells was observed (Figure 3a,b). In addition, we also incubated U87MG cells with LPAgNP conjugated c-RAD,[28] a widely used negative control peptide for c-RGD, and observed very little binding of the AgNPs to the cells (Figure 3c,d). With all these control studies, we could indeed attribute the high labeling efficiency of c-RGD-LPAgNPs to the high binding affinity of c-RGD peptides to $\alpha_v\beta_3$ integrin receptors. These results also indicated successful
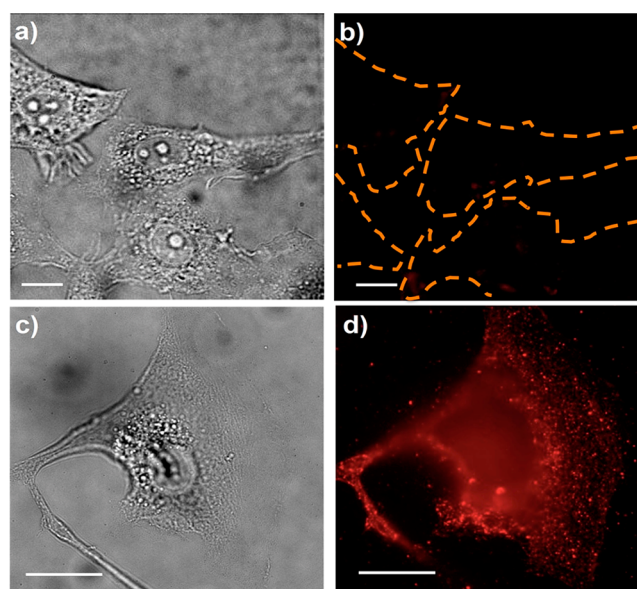

Figure 2. (a, b) Bright field and fluorescence images of fixed U87MG cancer cells incubated with 10 nM PEG-LPAgNPs. (c, d) Bright field and fluorescence images of fixed U87MG cancer cells incubated with 10 nM c-RGD-LPAgNPs. The scale bar of the images is 20 μm.
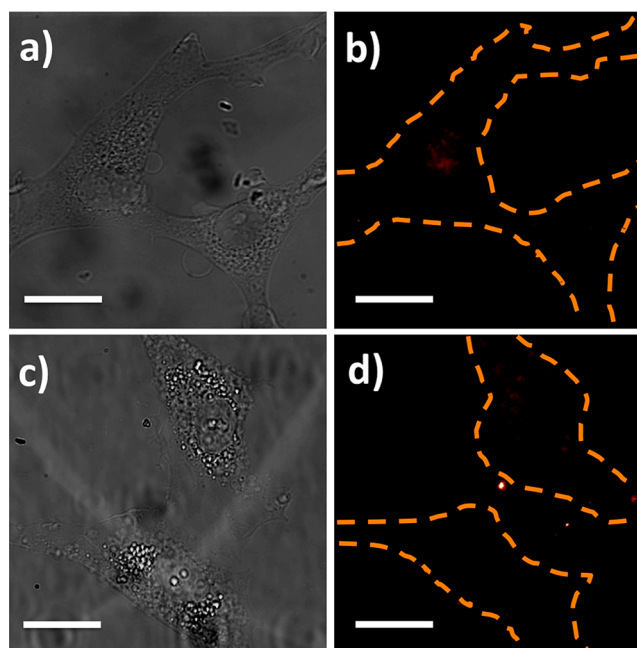

Figure 3. (a,b) Bright field and fluorescence images of c-RGD blocked U87MG cancer cells incubated with 10 nM c-RGD-LPAgNPs. (c,d) Bright field and fluorescence images of fixed U87MG cancer cells incubated with 10 nM c-RAD-LPAgNPs. The scale bar of the images is 20 μm.

conjugation of c-RGD to LPAgNPs, and the conjugated c-RGD peptides retained their high binding affinity and specificity to cancer receptors on the membrane.[29]

Once LPAgNPs (1 nM in MEM) were incubated with live U87MG cancer cells at 37 °C, the NPs were internalized by the cells, where the NPs were encapsulated in endosomes regardless of which types of ligands were on the surface. To gain a quantitative understanding of the differences in endocytosis kinetics between two types of LPAgNPs with
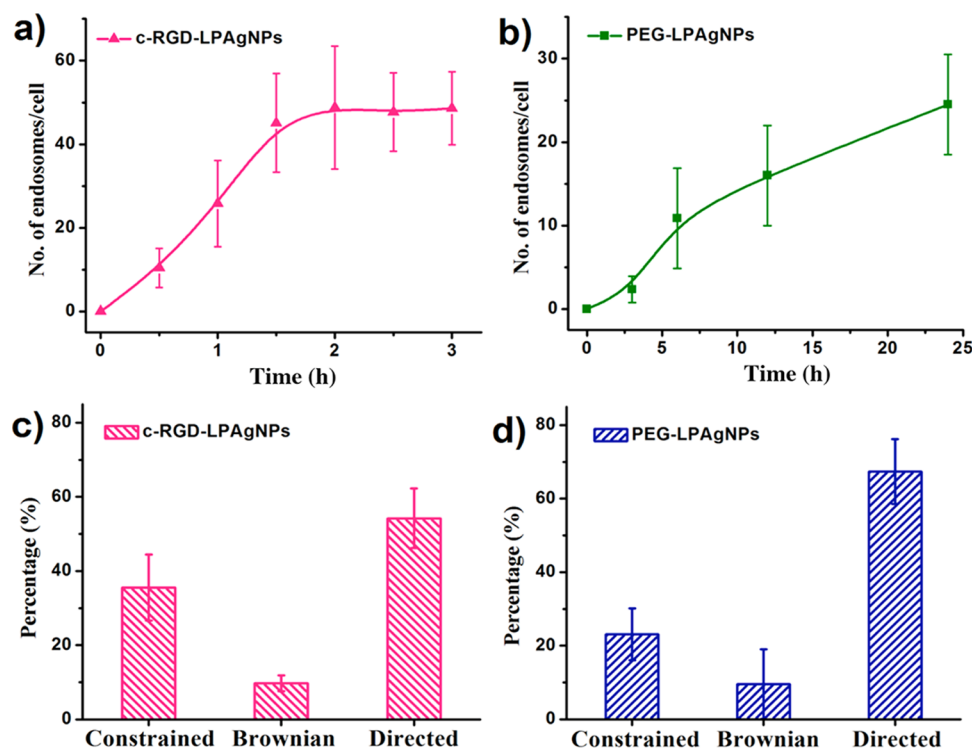
Figure 4. Cellular uptake kinetics of LPAgNPs. (a) Uptake kinetics of c-RGD-LPAgNPs in 3 h. (b) Uptake kinetics of PEG-LPAgNPs in 24 h. (c) Endosome cellular dynamics of c-RGD-LPAgNPs in U87MG cells. (d) Endosome cellular dynamics of PEG-LPAgNPs in U87MG cells.
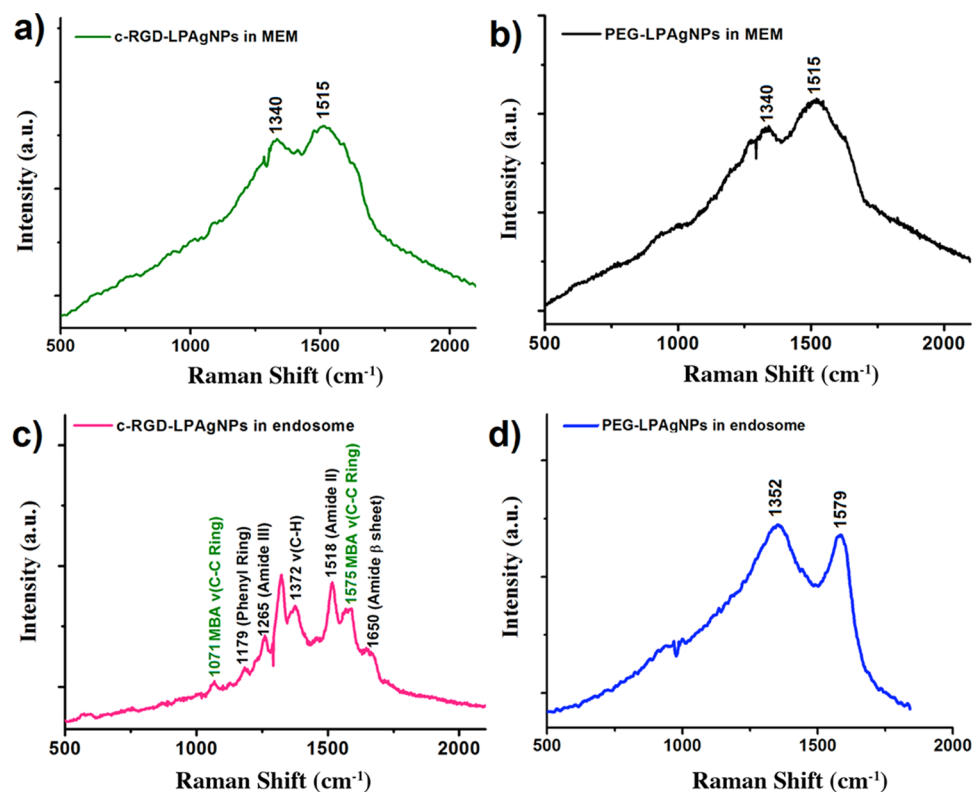

Figure 5. (a) Raman spectra of c-RGD-LPAgNPs in MEM. (b) Raman spectra of PEG-LPAgNPs in MEM. (c) Raman spectra of c-RGD-LPAgNPs in endosomes. (d) Raman spectra of PEG-LPAgNPs in endosomes.

different surface coatings, we used fluorescence microscopy to quantify the average number of endosomes at different incubation time points. The number of endosomes incubated with c-RGD-LPAgNPs reached a platform with 49 ± 9

endosomes observed at the first 3 h (Figure 4a and Figure S3b), while only very few endosomes (2−3) containing PEG-LPAgNPs were found inside cells during the same time period (Figure 4b and Figure S3a), suggesting the specific ligand−

receptor interactions played a key role in the internalization process of NPs.[8] With the increase of incubation time, the number of endosomes containing with PEG-LPAgNPs continues increased and reached 24 ± 6 in 24 h (Figure 4b), which was still 2 times lower than the number of endosomes induced by c-RGD ones (Figure 4a). The much faster endocytosis of c-RGD-LPAgNPs than the cellular uptake of PEG-LPAgNPs might be attributed to the decrease of localized Gibbs free energy induced by receptor−ligand interactions, which caused the membrane around the NPs to quickly wrap and form vesicle structures.[9,30] After internalization, the LPAgNPs with different surface ligands also exhibited distinct intracellular dynamics. Depending on the time exponent value derived from the correlation of log mean square displacement (MSD) versus log time lag $D = (1/4)(\Gamma\tau^{\alpha-1})$, where Γ is the transport coefficient, τ is the time lag, and α is the time exponent, the motion of endosomes can be divided into three categories according to the α value: directed motion due to the active transport ($\alpha > 1.1$), Brownian diffusion ($0.9 \leq \alpha \leq 1.1$), and constrained diffusion (particles are constrained in a limited area) ($\alpha < 0.9$).[31] After 3 h incubation, we found that ∼54% of endosomes encapsulated c-RGD-LPAgNPs showed directed motion while ∼10% and ∼36% of them showed Brownian diffusion and constrained diffusion, respectively (Figure 4c). On the other hand, ∼67% of endosomes encapsulated PEG-LPAgNPs exhibited directed motion, while ∼10% and ∼23% showed Brownian diffusion and constrained diffusion, respectively (Figure 4d). Significant increase in constrained diffusion observed from c-RGD-LPAgNPs indicated that the specific ligand−receptor interactions enhanced constrained diffusion of the NPs after internalized by the cells.

Strong Raman enhancements of these LPAgNPs also offered a unique opportunity to investigate the local chemical environment around the NPs before and after internalization. While characteristic Raman peaks were clearly observed from c-RGD-LPAgNPs and PEG-LPAgNPs in PBS solution (Figure 1e,f), these peaks were no longer distinguishable with only the same two bundled peaks at 1340 cm^{-1} and 1515 cm^{-1} observed in the presence of MEM cell culture media (Figure 5a,b) or PBS containing 10% FBS (v/v) (Figure S4). However, once the NPs were reseparated from those biomolecules through centrifugation purification, characteristic Raman vibrations of PEG, c-RGD, and MBA ligands on the particle surface were recovered (Figure S5). Such broadening in Raman spectra can be due to the significant interference from local amino acids and serum proteins in the media (the neighboring bands derived from amino acid residues and proteins are broad and appear in the same spectral region),[32−34] similar to the previous report by Tam et al.[3] Interestingly, once c-RGD-LPAgNPs were internalized into endosomes inside the cells, characteristic Raman vibrations at 1179, 1265, and 1518 cm^{-1} of c-RGD peptides were readily observed in individual endosomes again (Figure 5c). In contrast, the characteristic Raman vibrations of PEG-LPAgNPs and c-RAD-LPAgNPs remained indistinguishable after internalization (Figure 5d and Figure S6b). The interesting recovery of Raman signals of c-RGD-LPAgNPs in endosomes suggested that specific binding of c-RGD peptides to the $\alpha_v\beta_3$ integrin receptors potentially can minimize interference from local intracellular biological molecules.

In summary, by taking advantage of the synergy of bright and robust single-particle emission and strong Raman enhancements of LPAgNPs, we quantitatively investigated effects of two different well-known surface chemistries on cellular uptake and intracellular dynamics. Active targeting ligand, c-RGD, induced much more rapid cellular uptake than PEG due to the specific ligand−receptor interactions. Binding of c-RGD to $\alpha_v\beta_3$ integrin receptors on the cancer cells also increased the constrained diffusion of endosomes after internalization. More interestingly, specific ligand−receptor interactions also minimized interference from biomolecules in the local environment on Raman signals of c-RGD-LPAgNPs and resulted in recovery of specific c-RGD Raman vibrations inside endosomes, which potentially can be used to identify local specific ligand−receptor interactions at the chemical level inside live cells.

■ EXPERIMENTAL PROCEDURES

Synthesis of Luminescent Plasmonic Silver Nanoparticles (LPAgNPs). LPAgNPs were synthesized using the solid-state thermal reduction method we reported before.[21] 200 mg of glycine and 15 mg of silver nitrate were codissolved in 1.5 mL DI water. After the water evaporated, the mixture was then reduced at 453 K for 2 min in the solid state. When the color of the mixture became blackish, the reaction was stopped and the product was dissolved in 1 mL of DI water. The final solution was first centrifuged at 2000 and 4000 g for 2 min respectively to remove the large aggregates. LPAgNPs of ∼20 nm were obtained by collecting the pellets after centrifuging the supernatant at 7000 g for 3 min. The sample was further purified by centrifugation at 7000 g several times to remove the free ions and excess glycine ligands. The pellets were collected and redissolved in 10 mM sodium borate buffer for further study.

Bioconjugation of LPAgNPs. Mercaptobenzoic acid (MBA), as a ligand to serve as the internal standard of SERS studies, was dissolved in methanol solution (10 mM) and diluted to 1 mM using 10 mM sodium borate buffer. The conjugation of c-RGD peptides, cyclo (Arg-Ala-Asp-D-Phe-Cys) (c-RAD) peptides, or PEG molecules to LPAgNPs was conducted by incubating the LPAgNPs with MBA and c-RGD (c-RAD, PEG) at a molar ratio of $1:5 \times 10^4:5 \times 10^4$ in 10 mM sodium borate buffer for 2 h with gentle shaking. The excess ligands and free ions were removed by passing the sample through a Sephadex-20 column with PBS as elution phase. The sample was then centrifuged at 7000 g for 3 min and the pellets were redissolved in phosphate buffer saline (PBS) for further study.

Fixed Cell Labeling and Imaging. For cell labeling, U87MG cells were first fixed by 3.7% formaldehyde for 10 min. Then the fixative was removed and the cells were blocked with 1 mL 2 weight (wt) % BSA for 30 min. The fixed cells were incubated with 10 nM c-RGD-LPAgNPs, c-RAD-LPAgNPs, or PEG-LPAgNPs in 500 μL PBS buffer solution at room temperature for 45 min, respectively. The cells were then washed thoroughly with PBS buffer to remove the excess amount of NPs and used for imaging studies.

Blocking Study. U87MG cells were first fixed by 3.7% formaldehyde for 10 min. Then the fixative was removed and the cells were blocked with 1 mL 2 wt % BSA for 30 min. The fixed cells were incubated with 1 mM c-RGD in 500 μL PBS buffer solution at room temperature. After 45 min, the c-RGD was removed and the cells were washed thoroughly with PBS buffer for 3 times. Then the cells were incubated with 10 nM c-RGD-LPAgNPs for another 45 min before being used for cell imaging studies.

Cellular Endocytosis Studies. The live cells were incubated with 1 nM c-RGD-LPAgNPs in MEM for 0.5, 1,

1.5, 2, 2.5, and 3 h or with 1 nM PEG-LPAgNPs in MEM for 3, 6, 12, and 24 h at 37 °C, 5% CO_2. The cells at different time points were washed thoroughly with PBS buffer and used for cell imaging studies. Before the fluorescence cell images were taken, the cells were photobleached for 15 s. For each time point, the bright endosomes in each cell were localized and counted by Insight software developed by Dr. Bo Huang (Department of Pharmaceutical Chemistry and Department of Biochemistry and Biophysics, University of California, San Francisco). The size of the bright dots was chosen as larger than 50 pixels. Ten cells were analyzed at each time point and presented as mean ± SD ($n = 10$).

Cellular Dynamic Studies. The live cells incubated with c-RGD-LPAgNPs for 3 h and the live cells incubated with PEG-LPAgNPs for 24 h were used for the cellular dynamic studies, respectively. After 15 s photobleaching, fluorescence cell images were taken every 500 ms for 50 s. The Insight software was used for the localization and tracking of the bright dots (endosomes). The bright dot size was chosen as larger than 50 pixels. For the tracking study, the minimum trace length was 20 frames. The motions of the NPs were classified into three different modes according to the α (slope) value of the trajectories: constrained diffusion ($\alpha < 0.9$), Brownian diffusion ($0.9 \leq \alpha \leq 1.1$), and directed motion ($\alpha > 1.1$).[31]

Cellular SERS Studies. U87MG cancer cells were incubated with c-RGD-LPAgNPs or c-RAD-LPAgNPs for 3 h or with PEG-LPAgNPs for 24 h. The cells were washed thoroughly with PBS for 3 times after incubation to remove the excess amount of LPAgNPs. The Raman spectra were then collected with an Acton SP2300 (Princeton Instruments) under 532 nm excitation.

ASSOCIATED CONTENT

S Supporting Information

Materials and equipment, supplementary figures showing cellular study and Raman spectra. This material is available free of charge via the Internet at http://pubs.acs.org.

AUTHOR INFORMATION

Corresponding Author

*Tel: 972-883-5768; Fax: 972-883-2925; E-mail: jiezheng@ utdallas.edu.

Notes

The authors declare no competing financial interest.

ACKNOWLEDGMENTS

ABBREVIATIONS

PEG, polyethylene glycol; c-RGD, cyclo (Arg-Gly-Asp-D-Phe-Lys); SERS, surface-enhanced Raman scattering; LPAgNPs, luminescent plasmonic silver nanoparticles; QD, quantum dot; c-RAD, cyclo (Arg-Ala-Asp-D-Phe-Cys); MBA, mercaptobenzoic acid; TEM, transmission electron microscopy; DLS, dynamic light scattering; HD, hydrodynamic diameter; PBS, phosphate buffer saline; MEM, minimum essential media; FBS, fetal bovine serum; MSD, mean square displacement

REFERENCES

(1) Kim, S. T., Saha, K., Kim, C., and Rotello, V. M. (2013) The role of surface functionality in determining nanoparticle cytotoxicity. *Acc. Chem. Res. 46*, 681−691.

(2) Saha, K., Kim, S. T., Yan, B., Miranda, O. R., Alfonso, F. S., Shlosman, D., and Rotello, V. M. (2013) Surface functionality of nanoparticles determines cellular uptake mechanisms in mammalian cells. *Small 9*, 300−305.

(3) Tam, N. C., McVeigh, P. Z., MacDonald, T. D., Farhadi, A., Wilson, B. C., and Zheng, G. (2012) Porphyrin-lipid stabilized gold nanoparticles for surface enhanced Raman scattering based imaging. *Bioconjugate Chem. 23*, 1726−1730.

(4) Roxin, A., and Zheng, G. (2012) Flexible or fixed: a comparative review of linear and cyclic cancer-targeting peptides. *Future Med. Chem. 4*, 1601−1618.

(5) Gao, X. H., Cui, Y. Y., Levenson, R. M., Chung, L. W. K., and Nie, S. M. (2004) In vivo cancer targeting and imaging with semiconductor quantum dots. *Nat. Biotechnol. 22*, 969−976.

(6) Choi, H. S., Liu, W., Liu, F., Nasr, K., Misra, P., Bawendi, M. G., and Frangioni, J. V. (2010) Design considerations for tumour-targeted nanoparticles. *Nat. Nanotechnol. 5*, 42−47.

(7) Liu, J. B., Yu, M. X., Zhou, C., and Zheng, J. (2013) Renal clearable inorganic nanoparticles: a new frontier of bionanotechnology. *Mater. Today 16*, 477−486.

(8) Huang, X. H., Peng, X. H., Wang, Y. Q., Wang, Y. X., Shin, D. M., El-Sayed, M. A., and Nie, S. M. (2011) A reexamination of active and passive tumor targeting by using rod-shaped gold nanocrystals and covalently conjugated peptide ligands. *ACS Nano 5*, 6765−6765.

(9) Albanese, A., Tang, P. S., and Chan, W. C. (2012) The effect of nanoparticle size, shape, and surface chemistry on biological systems. *Annu. Rev. Biomed. Eng. 14*, 1−16.

(10) Zhang, J., Fu, Y., Conroy, C. V., Tang, Z. H., Li, G., Zhao, R. Y., and Wang, G. L. (2012) Fluorescence intensity and lifetime cell imaging with luminescent gold nanoclusters. *J. Phys. Chem. C 116*, 26561−26569.

(11) Luo, Z., Zheng, K., and Xie, J. (2014) Engineering ultrasmall water-soluble gold and silver nanoclusters for biomedical applications. *Chem. Commun.*, DOI: 10.1039/c3cc47512c.

(12) Fleischer, C. C., and Payne, C. K. (2012) Nanoparticle surface charge mediates the cellular receptors used by protein-nanoparticle complexes. *J. Phys. Chem. B 116*, 8901−8907.

(13) Cai, W. B., and Chen, X. Y. (2008) Preparation of peptide-conjugated quantum dots for tumor vasculature-targeted imaging. *Nat. Protoc. 3*, 89−96.

(14) Zhang, F., Huang, X. L., Zhu, L., Guo, N., Niu, G., Swierczewska, M., Lee, S., Xu, H., Wang, A. Y., Mohamedali, K. A., Rosenblum, M. G., Lu, G. M., and Chen, X. Y. (2012) Noninvasive monitoring of orthotopic glioblastoma therapy response using RGD-conjugated iron oxide nanoparticles. *Biomaterials 33*, 5414−5422.

(15) Zhen, Z. P., Tang, W., Chen, H. M., Lin, X., Todd, T., Wang, G., Cowger, T., Chen, X. Y., and Xie, J. (2013) RGD-modified apoferritin nanoparticles for efficient drug delivery to tumors. *ACS Nano 7*, 4830−4837.

(16) Iyer, A. K., Khaled, G., Fang, J., and Maeda, H. (2006) Exploiting the enhanced permeability and retention effect for tumor targeting. *Drug. Discovery Today 11*, 812−818.

(17) Wang, Y., Liu, Y., Luehmann, H., Xia, X., Brown, P., Jarreau, C., Welch, M., and Xia, Y. (2012) Evaluating the pharmacokinetics and in vivo cancer targeting capability of Au nanocages by positron emission tomography imaging. *ACS Nano 6*, 5880−5888.

(18) Liu, J., Yu, M., Ning, X., Zhou, C., Yang, S., and Zheng, J. (2013) PEGylation and zwitterionization: pros and cons in the renal clearance and tumor targeting of near-IR-emitting gold nanoparticles. *Angew. Chem., Int. Ed. Engl. 52*, 12572−12576.

(19) Brigger, I., Dubernet, C., and Couvreur, P. (2002) Nanoparticles in cancer therapy and diagnosis. *Adv. Drug. Delivery Rev. 54*, 631−651.

(20) Xie, J., Chen, K., Lee, H., Xu, C. J., Hsu, A. R., Peng, S., Chen, X. Y., and Sun, S. H. (2008) Ultrasmall c(RGDyK)-coated Fe_3O_4

nanoparticles and their specific targeting to integrin $\alpha_v\beta_3$—rich tumor cells. *J. Am. Chem. Soc. 130*, 7542−7543.

(21) Zheng, J., Ding, Y., Tian, B. Z., Wang, Z. L., and Zhuang, X. W. (2008) Luminescent and Raman active silver nanoparticles with polycrystalline structure. *J. Am. Chem. Soc. 130*, 10472−10473.

(22) Jin, Y. D., and Gao, X. H. (2009) Plasmonic fluorescent quantum dots. *Nat. Nanotechnol. 4*, 571−576.

(23) Zhou, C., Yu, J., Qin, Y. P., and Zheng, J. (2012) Grain size effects in polycrystalline gold nanoparticles. *Nanoscale 4*, 4228−4233.

(24) Jokerst, J. V., Lobovkina, T., Zare, R. N., and Gambhir, S. S. (2011) Nanoparticle PEGylation for imaging and therapy. *Nanomedicine (London) 6*, 715−728.

(25) Podstawka, E., Sikorska, E., Proniewicz, L. M., and Lammek, B. (2007) Raman and surface-enhanced Raman spectroscopy investigation of vasopressin analogues containing 1-aminocyclohexane-1 carboxylic acid residue. *Biopolymers 85*, 498−498.

(26) Yamini, D., Devanand Venkatasubbu, G., Kumar, J., and Ramakrishnan, V. (2014) Raman scattering studies on PEG functionalized hydroxyapatite nanoparticles. *Spectrochim. Acta., Part A 117*, 299−303.

(27) Orendorff, C. J., Gole, A., Sau, T. K., and Murphy, C. J. (2005) Surface-enhanced Raman spectroscopy of self-assembled monolayers: sandwich architecture and nanoparticle shape dependence. *Anal. Chem. 77*, 3261−3266.

(28) Miura, Y., Takenaka, T., Toh, K., Wu, S. R., Nishihara, H., Kano, M. R., Ino, Y., Nomoto, T., Matsumoto, Y., Koyama, H., Cabral, H., Nishiyama, N., and Kataoka, K. (2013) Cyclic RGD-Linked polymeric micelles for targeted delivery of platinum anticancer drugs to glioblastoma through the Blood-Brain tumor barrier. *ACS Nano 7*, 8583−8592.

(29) Kim, Y. H., Jeon, J., Hong, S. H., Rhim, W. K., Lee, Y. S., Youn, H., Chung, J. K., Lee, M. C., Lee, D. S., Kang, K. W., and Nam, J. M. (2011) Tumor targeting and imaging using cyclic RGD-PEGylated gold nanoparticle probes with directly conjugated iodine-125. *Small 7*, 2052−2060.

(30) Gao, H. J., Shi, W. D., and Freund, L. B. (2005) Mechanics of receptor-mediated endocytosis. *Proc. Natl. Acad. Sci. U. S. A. 102*, 9469−9474.

(31) Feder, T. J., Brust-Mascher, I., Slattery, J. P., Baird, B., and Webb, W. W. (1996) Constrained diffusion or immobile fraction on cell surfaces: a new interpretation. *Biophys. J. 70*, 2767−2773.

(32) Callender, R., and Deng, H. (1994) Nonresonance Raman difference spectroscopy: a general probe of protein structure, ligand binding, enzymatic catalysis, and the structures of other biomacromolecules. *Annu. Rev. Biophys. Biomol. Struct. 23*, 215−245.

(33) Yonzon, C. R., Haynes, C. L., Zhang, X., Walsh, J. T., Jr., and Van Duyne, R. P. (2004) A glucose biosensor based on surface-enhanced Raman scattering: improved partition layer, temporal stability, reversibility, and resistance to serum protein interference. *Anal. Chem. 76*, 78−85.

(34) Xie, Y., Jiang, Y., and Ben-Amotz, D. (2005) Detection of amino acid and peptide phosphate protonation using Raman spectroscopy. *Anal. Biochem. 343*, 223−230.